remote sensing

MDPI

Article

Weak Signal Processing Method for Moving Target of GNSS-S Radar Based on Amplitude and Phase Self-Correction

Wenning Gao [1,2], Fuzhan Yue [1,2,*], Zhenghuan Xia [1,2], Xin Liu [1,2], Chuang Zhang [1,2], Zongqiang Liu [1,2], Shichao Jin [1,2], Yao Zhang [1,2], Zhilong Zhao [1,2], Tao Zhang [1,2] and Ying Zhang [1,2]

[1] State Key Laboratory of Space-Earth Integrated Information Technology, Beijing 100095, China
[2] Beijing Institute of Satellite Information Engineering, Beijing 100095, China
* Correspondence: yuefzh@163.com; Tel.: +86-10-68197402

Abstract: Navigation satellite signals have the advantages of all-day, all-weather, and global coverage, and the use of navigation signals for the detection of moving targets has significant application prospects. However, the GNSS signal is very weak, and the signal power is greatly attenuated after being scattered by the target. In order to detect the echo signal, a long integration time is required. However, the movement of the target will cause the echo signal to produce unpredictable range migration and a Doppler frequency shift, which will weaken the cumulative effect of long-term integration. This paper proposes a weak signal processing method with amplitude and phase self-correction for moving target detection in the GNSS-S radar. First, the phase consistency of the echoes of a single GNSS satellite is realized by the block expansion compression and phase differential correction method to improve the coherent accumulation gain; then, multi-star joint accumulation is carried out after the signal amplitudes of multiple satellites are corrected by the improved keystone method, so as to obtain a stable echo signal track. This method can effectively improve the integral gain of the scattering signal of the moving target and realize target detection. The simulation results and field tests show that this method can effectively improve the SNR of the GNSS-S signal and can realize the detection of small moving targets such as cars with GNSS-S radar.

Keywords: GNSS-S radar; moving target detection; long-term coherent processing; weak signal

Citation: Gao, W.; Yue, F.; Xia, Z.; Liu, X.; Zhang, C.; Liu, Z.; Jin, S.; Zhang, Y.; Zhao, Z.; Zhang, T.; et al. Weak Signal Processing Method for Moving Target of GNSS-S Radar Based on Amplitude and Phase Self-Correction. *Remote Sens.* **2023**, *15*, 969. https://doi.org/10.3390/rs15040969

Academic Editor: Mohammad Zahidul Hasan Bhuiyan

Received: 15 December 2022
Revised: 1 February 2023
Accepted: 8 February 2023
Published: 9 February 2023

1. Introduction

GNSS-S (Global Navigation Satellite System-Scattering) uses the signal of the GNSS satellite as the radiation source and realizes the detection and perception of the target by receiving the backscatter signal of the GNSS from the target. This technology is widely used in ground object recognition, surface deformation monitoring, ocean wind waves, soil moisture inversion, etc. [1]. Compared with traditional GNSS-R technology, GNSS-S gets rid of the limitation of specular reflection points, has a higher information dimension and a larger detection width, and can extract more abundant feature information to improve the fineness of detected targets. Because GNSS-S detection technology can realize large and wide observation of ocean and land, and has the advantages of low cost, anti-interference, and strong concealment [2], it has broad application prospects.

In recent years, GNSS-based passive radar has aroused great interest of researchers and they have carried out a lot of research, but most of them focus on the detection of static objects on land or large slow-moving targets such as large cruise ships. Due to the extremely weak power of navigation signals, research on small targets or fast-moving targets is still relatively rare. Paper [3] proposed the concept of using GNSS signals for maritime target detection and proved its feasibility through experiments. Paper [4] analyzes the signal chain of GNSS as a non-cooperative radiation source for SAR detection and points out that limited by the weak signal power of GNSS, long-term integration is required to achieve target detection. In the literature [5,6], a long-term accumulation method is

proposed to improve the target echo signal power, in order to realize GNSS passive radar detection and solve the problem of extremely weak GNSS signal power. However, during the long-term observation process, the motion of the target cannot be ignored, which will cause the range migration and Doppler frequency shift of the target echo signals. In the literature [7], a mixed mode of coherent accumulation and non-coherent accumulation is proposed to solve the influence of signal Doppler frequency shift. However, due to the square loss of non-coherent accumulation, the signal gain improvement is limited. In the literature [8], the Doppler and range migration of the target motion are compensated to improve the SNR of the echo signal, but the realization method is to use post-event manual compensation for GEO satellites in geostationary orbit. In the field of radar, the traditional methods to achieve long-term coherent accumulation of moving targets mainly include fractional Fourier transform [9], Radon Fourier transform [10], and Radon fractional Fourier transform [11,12]. However, the computational complexity of these methods is very high, and because the GNSS signal is a continuous signal, the amount of data is much larger than that of the pulse signal, and therefore more efficient computational methods need to be explored. Furthermore, when it comes to the GNSS-S radar, since the landing power of the navigation signal is only 130 dBm [13], the power of the signal scattered by the target is even lower. A longer accumulation time is required to achieve target detection, so the consistency of the amplitude and phase of the signal has to be considered. In addition, the structure of the GNSS signal is mainly used for information transmission, and the PRN codes and navigation message bits are modulated on the carrier [14], which will cause random changes in the phase of the received signal. It is very difficult to achieve long-term coherent accumulation [15]. In addition, GNSS-based radar is a bistatic configuration with separate transceivers [16], and the RCS of the target is related to the position of the GNSS satellite, the position of the receiver, and the bistatic angle [17,18]. The bistatic RCS of the target will change randomly during the movement, resulting in fluctuations in the echo signal intensity of a single navigation satellite [19,20]. Therefore, the moving target detection technology based on an active radar system is not suitable for the GNSS-S radar.

Aiming at the problem that the GNSS-S signal is extremely weak and the bistatic RCS of the moving target changes randomly during the movement process, a multi-satellite joint accumulation method with amplitude and phase self-correction is proposed. Firstly, by expanding and compressing the GNSS-S signal in blocks, the influence of satellite Doppler frequency shift and random phase reversal caused by navigation message bits is eliminated, so as to improve the coherent accumulation gain of a single satellite. Then, the signal amplitude correction is performed on the two-dimensional echo signals of multiple navigation satellites, and the weighted fusion of the multi-satellite echo signals is carried out.

The subsequent structure of the paper is as follows: the second section introduces the GNSS-S radar detection system; the third section describes the processing process of the amplitude and phase self-correction method; the fourth section gives the theoretical simulation and field test results; and finally, the fifth section gives some conclusions of this paper.

2. Overview of GNSS-S Radar System

2.1. System Composition

The GNSS-S radar system involved in this paper uses GNSS satellites as the radiation source and realizes target detection through the GNSS-S signal scattered by the target. The system composition is shown in Figure 1. It mainly includes three parts: the direct receiving antenna, the scattering receiving antenna, and the receiving and processing host. The main technical parameters are shown as Table 1. The direct receiving antenna points to the zenith, receives the direct signal from the GNSS satellite, and the scattering receiving antenna points to the direction of the detection target. The receiving and processing host completes the synchronous reception of the direct and scattering signals and executes the corresponding detection processing algorithm.

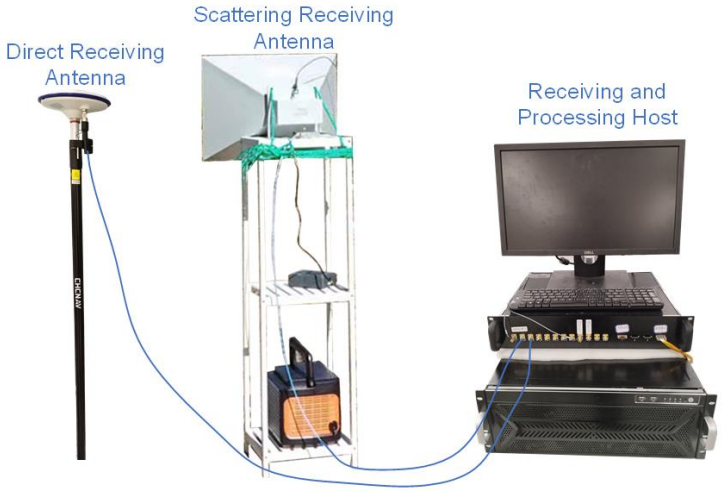

Figure 1. Composition Diagram of GNSS-S Radar System.

Table 1. Main parameters of the system.

Item	Parameter
Gain of direct receiving antenna	3 dBi
Gain of scattering receiving antenna	15 dBi
Working frequency	BDS B3: 1268.52 MHz
Beam width of scattering receiving antenna	±13°
Sampling rate	200 MSPS
Storage capacity	1 TB
power	200 W

2.2. Geometry Configuration

The geometric structure of the system is shown in Figure 2. The distance from the GNSS satellite i to the receiver is D_i, the signal propagation distance from the ground moving target to the receiver is $R_i + R_i'$, and the bistatic angle composed of satellite, target, and receiver is α_i. The propagation path difference between the direct signal and scattering signal ΔR_i is shown in Formula (1).

$$\Delta R_i = R_i + R_i' - D_i \tag{1}$$

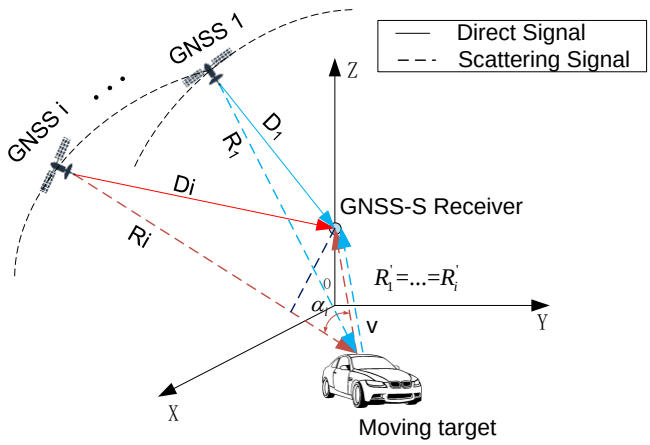

Figure 2. System Geometry.

The path difference at the initial moment of detecting the target is denoted as ΔR_0, The radial velocity between the target and the receiver is denoted as v. Considering that

the position of GNSS satellites changes very little during the detection period, the change in ΔR is mainly caused by the target motion, so it can be expressed in the form of Formula (2). The time difference of signal propagation caused by this path difference is Δt, as shown in Formula (3), where c is the propagation speed of an electromagnetic wave, which is 3×10^8 m/s.

$$\Delta R \approx \Delta R_0 - \mathrm{v} \cdot t \tag{2}$$

$$\Delta t = \frac{\Delta R(\mathrm{t})}{c} \approx \frac{\Delta R_0 - \mathrm{v} \cdot t}{c} \tag{3}$$

2.3. Signal Model

The GNSS signal model is shown in Formula (4), which adopts the modulation mode of code division multiple access, and the signal is composed of "PRN codes + navigation message bits" modulated on the carrier [21].

$$s_{\mathrm{d}}(t) = A \cdot D(t) \cdot C(t) \cdot \cos(2\pi f_c t + \phi) \tag{4}$$

where A, $D(t)$, $C(t)$, f_c, and ϕ are signal amplitude, navigation message bit, PRN code, carrier frequency, and carrier initial phase, respectively.

According to the geometric configuration of the GNSS-S system given in Figure 2, the scattering signal model is expressed as Formula (5).

$$s_{\mathrm{r}}(t) = A \cdot D(t - \Delta t) C(t - \Delta t) \cos\left[2\pi f_c'(t - \Delta t) + \phi\right] \tag{5}$$

where f_c' is the signal Doppler caused by the relative motion of the satellite and the target, and Δt is the time difference in Formula (3). When the distance between the receiver and the target is much smaller than the distance between the GNSS satellite and the target, $f_c' \approx f_c$.

After removing the carrier frequency by quadrature demodulation, the expressions of the direct signal and the scattered signal become Formulas (6) and (7).

$$s_{\mathrm{d}}(t) = A \cdot D(t) \cdot C(t) \cdot \mathrm{e}^{j*\phi} \tag{6}$$

$$s_{\mathrm{r}}(t) = A \cdot D(t - \Delta t) \cdot C(t - \Delta t) \cdot \exp\{-j \cdot 2\pi f_c \Delta t + \phi\} \tag{7}$$

3. Phase and Amplitude Self-Correction Processing Methods

Different from the chirp signal of traditional synthetic aperture radar, the GNSS signal is a continuous signal of code division multiple access, which is modulated with pseudo-random noise code and navigation message bits. In order to carry out long-term coherent accumulation and improve the processing gain of extremely weak signals, this paper proposes a phase-amplitude self-correction method to realize long-term coherent accumulation of scattering signals of moving targets.

The processing flow of this method is shown in Figure 3, including three steps. Firstly, the direct signal and scattering signal are blocked, expanded, and compressed. The signal is compressed within a code period into a data block, and different data are arranged in blocks in columns to form a slow-time and fast-time 2-D data matrix. Then, the phase of the signal is corrected by the phase differential method for each column of data, so that the phase of each column of the signal remains consistent. Finally, the amplitude correction is performed on the data sets of each satellite to eliminate the signal amplitude difference between different satellites, and the data sets of multiple satellites are jointly accumulated to obtain a continuous target echo signal map to realize the detection of moving targets.

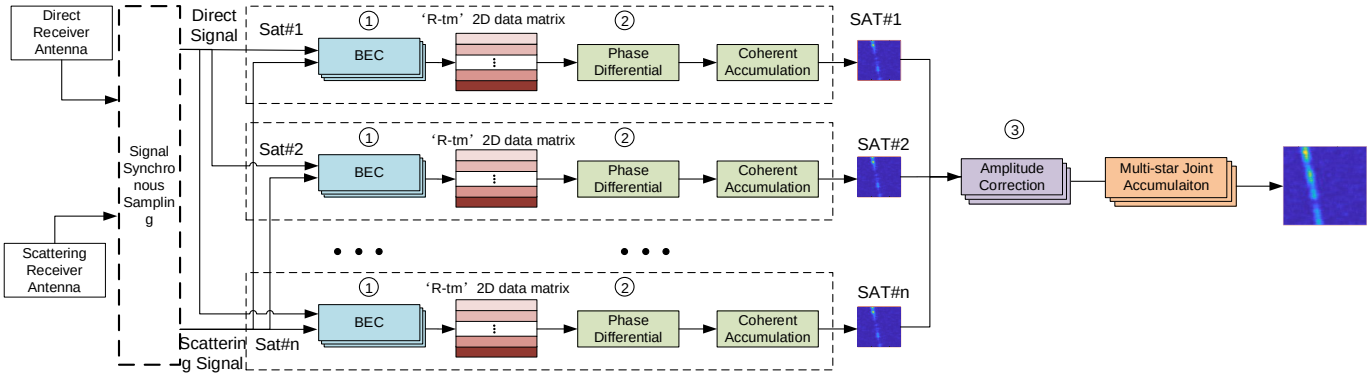

Figure 3. Signal Processing Flowchart.

3.1. Block Expended Compression

The GNSS-S signal is a one-dimensional time series signal, which needs to be converted into a two-dimensional time–distance domain signal through the Block Extended Compression (BEC) method. In addition, the effects of satellite Doppler and navigation message bits need to be removed.

As shown in Figure 4, the BEC algorithm is mainly divided into three steps, that is, signal block, carrier and PRN code stripping, and stripping of message bits. Firstly, the one-dimensional time series signal is divided into several data blocks with the same length according to the starting moment of the code period of the direct signal for correlation calculation. However, due to the different propagation paths of the scattered echo signal and the direct signal, there is a deviation in the code phase, and the Doppler frequency shift caused by the target movement will also cause the stretching effect of the scattered echo code period, destroying the periodicity of the PRN codes. In the method, two adjacent blocks are spliced together to improve the correlation gain of the PRN codes.

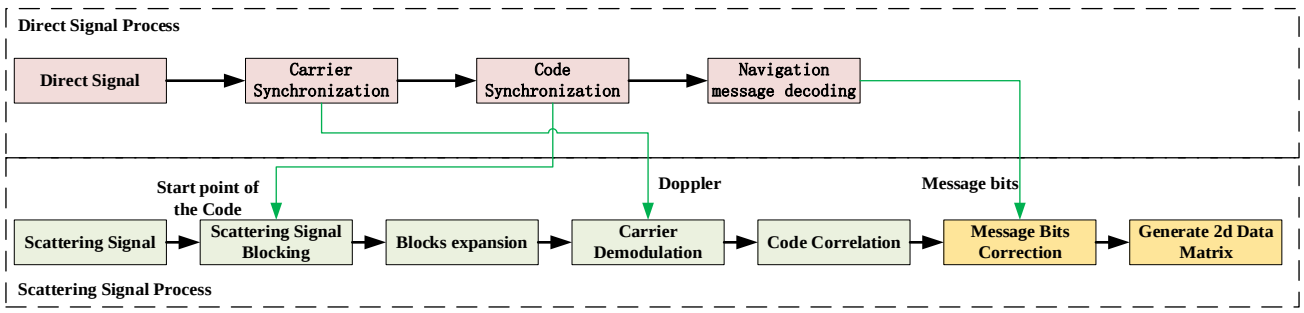

Figure 4. BEC algorithm flow chart.

Step 1: Direct signal processing. Receive direct navigation satellite signals, implement carrier synchronization and pseudo-random code synchronization, output direct satellite Doppler and code cycle start signals, complete navigation message analysis, and output information of message bits.

Step 2: Block the scattering signal. Including block operation and expansion operation, as shown in Figures 5 and 6.

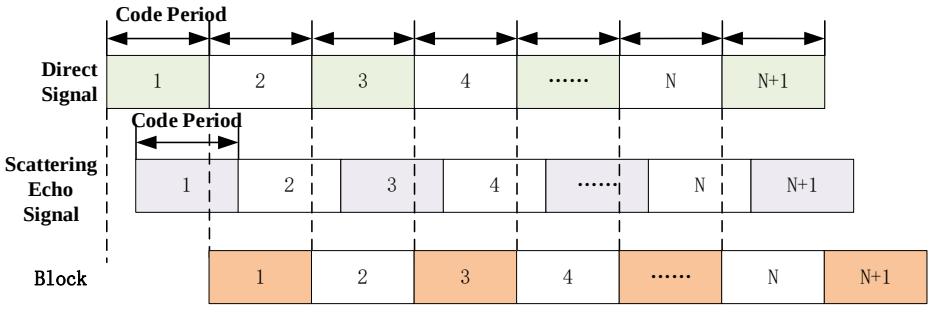

Figure 5. Schematic diagram of block operation.

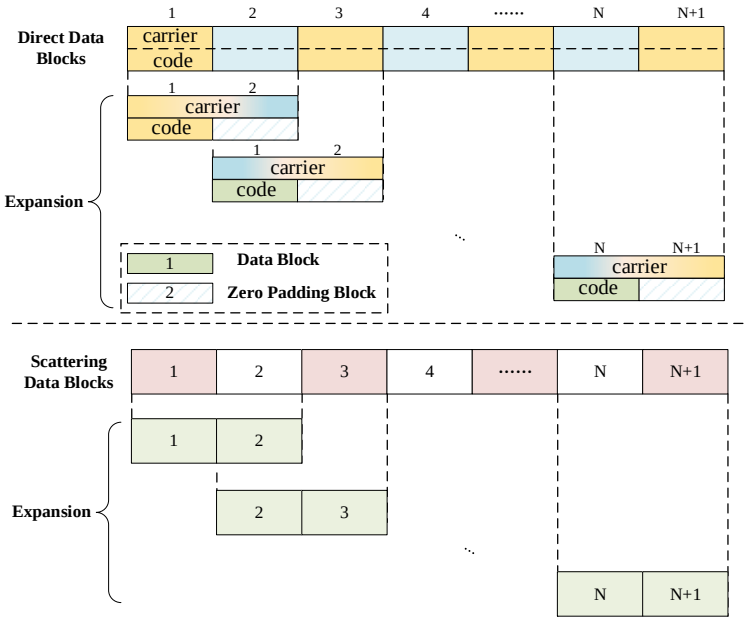

Figure 6. Schematic diagram of expansion operation.

(a) Block operation: First, track the direct navigation satellite signal in real time, implement the separation of direct signal carrier and PRN code, and generate a copy of the direct signal carrier data block and PRN code data block. The block length of the data block is one PRN code period. For example, the code period of the BDS B3 is 1 ms, and the length of the direct signal data block is 1 ms. Then, the scattering echo signal is divided into blocks according to the initial moment of each code period of the direct signal, and the block length remains the same as that of the corresponding block of the direct signal.

(b) Expansion operation. The expansion of the copy signal of the direct signal is divided into two parts. One is to splice two adjacent carrier data sub-blocks; the other is to add zero blocks to each sub-block of the PRN block, the length of which is the same as the next sub-block. The expansion of the scattered echo signal is to splice every two adjacent sub-blocks together to form a new data block.

Step 3: Scattering signal compression. The Schematic diagram of data compress is shown in Figure 7. First, the scattering data block is mixed with the direct carrier data block, the carrier of the scattering signal is stripped, and then correlated with the direct PRN block. Perform FFT transformation on the echo data after frequency mixing and transfer the data to the frequency domain; first, perform FFT on the expanded PRN block, and then convert it to complex conjugate, and multiply the obtained frequency domain data with the echo signal in the frequency domain. Then, perform IFFT transformation on the data, and remove the first half of the data after returning to the time domain. This is the data compression process.

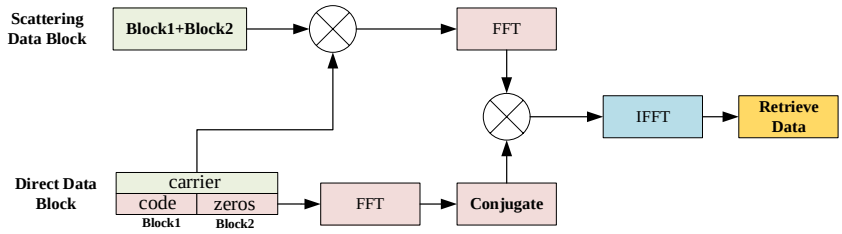

Figure 7. Schematic diagram of data compress.

The scattered signal forms two-dimensional data after BEC, and the expression is as follows:

$$\begin{aligned} s_{\mathrm{r}}(t_m, t) &= A \cdot D(t-\Delta t) \cdot X(t-\Delta t) \cdot \exp\{-j \cdot 2\pi f_c \Delta t\} \\ &= A \cdot D(t - \tfrac{\Delta R_0 - \mathrm{v} \cdot t_m \cdot (1+\cos(\alpha_i))}{c}) \cdot X\left(t - \tfrac{\Delta R_0 - \mathrm{v} \cdot t_m \cdot (1+\cos(\alpha_i))}{c}\right) \\ &\quad \cdot \exp\left\{-j \cdot 2\pi f_c \tfrac{\Delta R_0 - \mathrm{v} \cdot t_m \cdot (1+\cos(\alpha_i))}{c}\right\} \end{aligned} \tag{8}$$

where t_m denotes slow time; t denotes fast time; A is the amplitude envelope of the signal; $D(\cdot)$ denotes navigation message bits; $X(\cdot)$ represents the self-correlation function of PRN codes; α_i denotes the double station angle; c denotes the propagation speed of electromagnetic wave; and j denotes the imaginary unit.

According to the message bits obtained from the direct signal, the data phase inversion caused by the message bit inversion in the two-dimensional data is eliminated, and the data expression is as in formula (9).

$$s_{\mathrm{r}}(t_m, t) = A \cdot X\left(t - \frac{\Delta R_0 - \mathrm{v} \cdot t_m \cdot (1+\cos(\alpha_i))}{c}\right) \cdot \exp\left\{-j \cdot 2\pi f_c \frac{\Delta R_0 - \mathrm{v} \cdot t_m \cdot (1+\cos(\alpha_i))}{c}\right\} \tag{9}$$

3.2. Phase Differential Alignment

Since the target scattering signal is very weak, the signal after BEC is still very weak. In order to find the target echo signal, it is necessary to further perform long-term coherent accumulation on the compressed data block. By analyzing the phase part in Equation (9), the exponential term $\exp\left\{-j \cdot 2\pi f_c \frac{\Delta R_0 - \mathrm{v} \cdot t_m \cdot (1+\cos(\alpha_i))}{c}\right\}$, it is found that in the slow time tm direction, due to the existence of the target radial velocity v, the signal phase changes continuously with the slow time tm, which will affect the coherence cumulative effect.

In this paper, the phase differential method is used to achieve phase alignment. It can be seen from Formula (9) that the signal phase is shown in Formula (10).

$$\theta(t_m) = 2\pi f_c \frac{\Delta R_0 - \mathrm{v} \cdot t_m \cdot (1+\cos(\alpha_i))}{c} \tag{10}$$

The initial velocity of the target movement is v_0, the acceleration is a, and the velocity can be represented as $v = v_0 + a \cdot t_m$.Then, the signal phase can be written as Formula (11).

$$\theta(t_m) = 2\pi f_c \frac{\Delta R_0 - (\mathrm{v}_0 \cdot t_m + \mathrm{a} \cdot t_m^2) \cdot (1+\cos(\alpha_i))}{c} \tag{11}$$

Since the phase of noise is random, the phase of signal is shown in Formula (11), which is a function of slow time t_m. After calculating the second derivative of t_m in Formula (11), the signal phase is transformed into Formula (12), thereby eliminating the influence of velocity v, that is, offsetting the phase change caused by the target motion. The transformed signal model is shown in Formula (13).

$$\Delta\theta(t_m) = -4\pi f_c a \cdot (1+\cos(\alpha_i)) \tag{12}$$

$$\Delta s_{\mathrm{r}}(t_m, t) = A \cdot X\left(t - \frac{\Delta R_0 - \mathrm{v} \cdot t_m \cdot (1 + \cos(\alpha_i))}{c}\right) \cdot \exp\{-j4\pi f_c a \cdot (1 + \cos(\alpha_i))\} \quad (13)$$

3.3. Amplitude Correction

From the term $X\left(t - \frac{\Delta R_0 - \mathrm{v} \cdot t_m \cdot (1+\cos(\alpha_i))}{c}\right)$ in Formula (13), it can be seen that due to the existence of the target motion velocity v, the signal amplitude envelope $X(.)$ will undergo distance migration along with the slow time tm. In addition, due to the different positions and bistatic angles of GNSS satellites, the starting position and slope of the signal amplitude migration are also different, as shown in Figure 8.

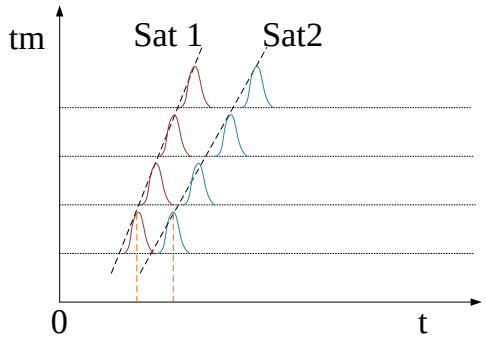

Figure 8. Amplitude migration of different satellites.

The correction of the slope of the distance migration is realized through the improved keystone transformation: Firstly, the FFT transformation is performed on Formula (9) along the fast time t dimension, which forms Formula (14), where A′ is the signal amplitude after FFT transformation. It can be seen from the second term of the above formula that t_m and f are coupled.

$$\begin{aligned} s_{\mathrm{r}}(t_m, f) &= A' \cdot \exp\left\{-j2\pi f \frac{\Delta R_0 - \mathrm{v} \cdot t_m \cdot (1+\cos(\alpha_i))}{c}\right\} \cdot \exp\left\{-j2\pi f_c \frac{\Delta R_0 - \mathrm{v} \cdot t_m \cdot (1+\cos(\alpha_i))}{c}\right\} \\ &= A' \cdot \exp\left\{-j2\pi (f + f_c) \frac{\Delta R_0}{c}\right\} \exp\left\{j2\pi (f + f_c) \frac{\mathrm{v} \cdot t_m \cdot (1+\cos(\alpha_i))}{c}\right\} \end{aligned} \quad (14)$$

Then, the transformation Formula (15) is substituted into Formula (14), that is, the slow-time axis is scaled according to the fast-time frequency and the bistatic angle of the satellite. The decoupled slow time–frequency domain signal is shown in Formula (16), which realizes the decoupling of t_m and f.

$$t'_m = \frac{f + f_{\mathrm{c}}}{f_c} t_m \cdot (1 + \cos(\alpha_i)) \quad (15)$$

$$s_{\mathrm{r}}(t'_m, f) = A' \cdot \exp\left\{-j2\pi (f + f_c) \frac{\Delta R_0}{c}\right\} \exp\left\{j2\pi f_c \frac{\mathrm{v} \cdot t'_m}{c}\right\} \quad (16)$$

IFFT transformation is performed on Formula (16) in the fast time dimension and converted into Formula (17). It can be seen that the influence of velocity v and the bistatic angle of the satellite on the amplitude migration is removed from the amplitude item, and the correction of the signal amplitude slope is realized.

$$s_{\mathrm{r}}(t'_m, t) = A \cdot X\left(t - \frac{\Delta R_0}{c}\right) \cdot \exp\left\{-j2\pi f_c \frac{\Delta R_0 - \mathrm{v} \cdot t'_m}{c}\right\} \quad (17)$$

The correction of the initial distance difference ΔR_0 is performed by compensating the public error term, which is obtained by calculating the distance difference of each satellite at the initial moment of detection. Formula (18) is obtained after correction.

$$s_{\mathrm{r}}(t'_m, t) = A \cdot X(t) \cdot \exp\left\{-j2\pi f_c \frac{-\mathrm{v} \cdot t'_m}{c}\right\} \tag{18}$$

Finally, weighted accumulation is performed on the signal data of different satellites, as shown in Formula (19), where P_i is the weight value of the i-th GNSS satellite. The selection of the weight value is based on the signal intensity of each satellite, so as to realize the compatible fusion of strong and weak signals.

$$\Delta S = \sum_{i=1}^{N} \left|\Delta s_{\mathrm{ir}}(t'_m, t)\right| \cdot P_i = \sum_{i=1}^{N} |A \cdot X(t)| \cdot P_i \tag{19}$$

4. Results

4.1. Simulated Results

In order to verify the effectiveness of the proposed method, simulations are carried out in this section and compared with traditional coherent accumulation and non-coherent accumulation methods. During the simulation, the original signal is generated according to the signal format of the navigation satellite, and Gaussian white noise is added as the background interference. The simulation system uses the navigation satellite signal of BDS B3, and the number of simulated satellites is two. The signal center frequency is 1268.52 MHz, which is mixed to 148.52 MHz through the RF front-end, and the sampling frequency fs is 200 MHz. According to the official ICD document of the BDS navigation system, the power of the signal reaching the ground is −130 dBm, and the bandwidth of the B3 signal is 10.23 MHz. Therefore, the SNR of the simulation signal is selected as a typical value of −30 dB. The detailed parameters are shown in Table 2.

Table 2. Simulation conditions.

Item	Parameter
Signal type	BDS B3
Carrier frequency	1268.52 MHz
Code frequency	10.23 MHz
PRN code period	1 ms
SNR	−30 dB
Target motion speed	0~100 m/s
Target motion acceleration	0~15 m/s^2

Using the block expansion compression algorithm in Section 3.1, the target echo signal is preprocessed, and the data blocks are arranged vertically in the form of one data block per PRN period. Then, the original image after data compression is obtained as shown in Figure 9. In order to analyze the signal phase relationship, a slightly higher SNR is used in the simulation, and the signal track can be seen in Figure 9.

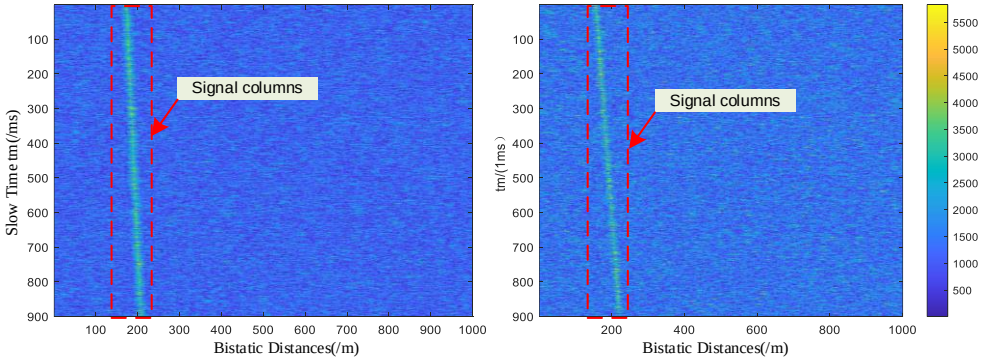

(**a**) (**b**)

Figure 9. Target echo signal diagram of satellite 1 (**a**) and satellite 2 (**b**).

The signal column in the original data is selected, and the signal phase change relationships are analyzed as shown in Figure 10a. Due to the existence of the moving speed of the target, the signal phase changes continuously with the slow time t_m between $\pm 180°$, so it is impossible to directly carry out coherent accumulation between each piece of data.

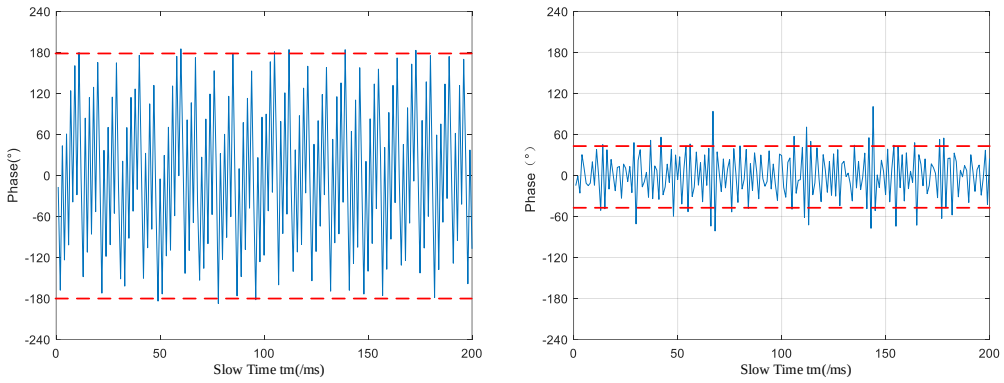

(**a**) Before phase correction (**b**) After phase correction

Figure 10. Signal phase diagrams before and after correction.

Then, the signal phase is corrected according to the phase differentiation method in Section 3.2. The corrected signal phase is shown in Figure 10b. The variation range of the signal phase is basically maintained within the range of $\pm 45°$, which realizes the consistency of the signal phase.

The phase-corrected signals are coherently accumulated to obtain a two-dimensional map in the "time-distance domain", as shown in Figure 11. Compared with Figure 9, the SNR of the signal has been greatly improved.

It can also be seen from Figure 11 that with the movement of the target, the amplitude of the signal energy migrates along the distance dimension, and the signal energy is not in the same column. In addition, because of the different geometric configurations of different GNSS satellites, the starting point and slope of the echo signal amplitude migration are also different. According to the amplitude correction method in Section 3.3, the echo signal amplitude is corrected. The corrected image is shown in Figure 12. The signal trajectory becomes vertical, and the starting point is kept aligned, so that the signal amplitude is consistent on the vertical axis. Finally, the echo signals of multiple GNSS satellites are jointly accumulated to obtain the multi-satellite fusion target echo map. As shown in Figure 12, the distance migration of the signal is corrected, and the SNR is also improved.

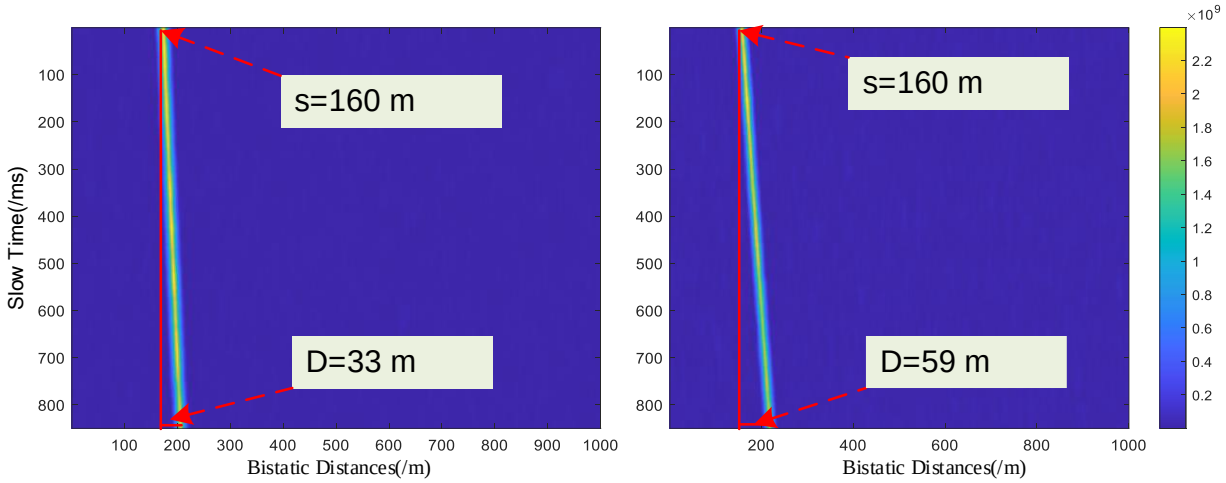

(**a**) Satellite 1 (**b**) Satellite 2

Figure 11. The target "time-distance domain" signal map by accumulating the phase-corrected data.

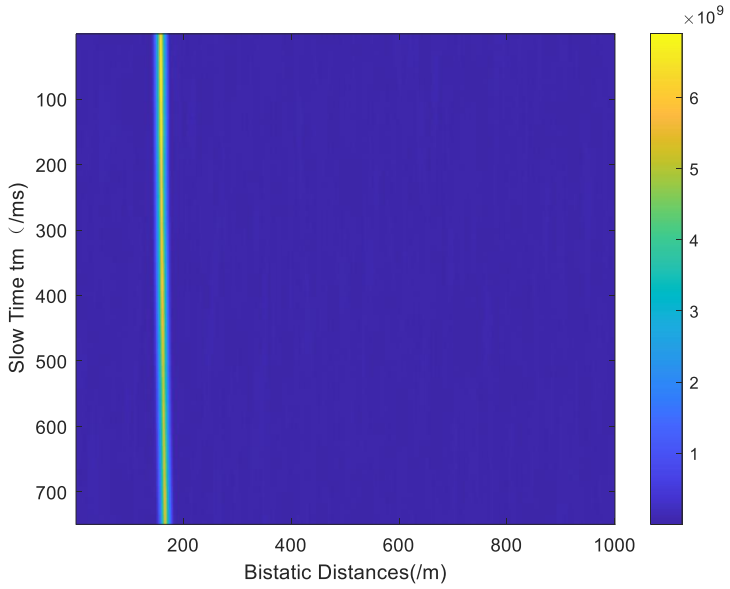

Figure 12. Signal Accumulation Result after Amplitude Correction.

4.2. Field Experimentation

In order to further prove the effectiveness of the proposed method, field experimentation was carried out in Beijing Environmental Science and Technology Park using the experimental equipment shown in Figure 1, and the BDS satellite B3 frequency band signal was selected as the signal transmission source. The direct receiving antenna adopts a circular omnidirectional receiving antenna, and the scattering receiving antenna adopts a high-gain horn antenna. Both direct and scattering signals are connected to the signal processing host to realize multi-channel synchronous data collection. Figure 13 is a diagram of the experimentation site. The detection equipment was erected on the side of the road to detect passing cars.

Figure 13. Experimental site scene.

Figure 14 shows the distribution and relative position of the BDS satellites received at the test site. With the location of the receiver as the center, the car passed by at high speed from south to north, and eight typical satellites constituting the backscatter were selected as radiation sources for detection. Satellite information is shown in Table 3.

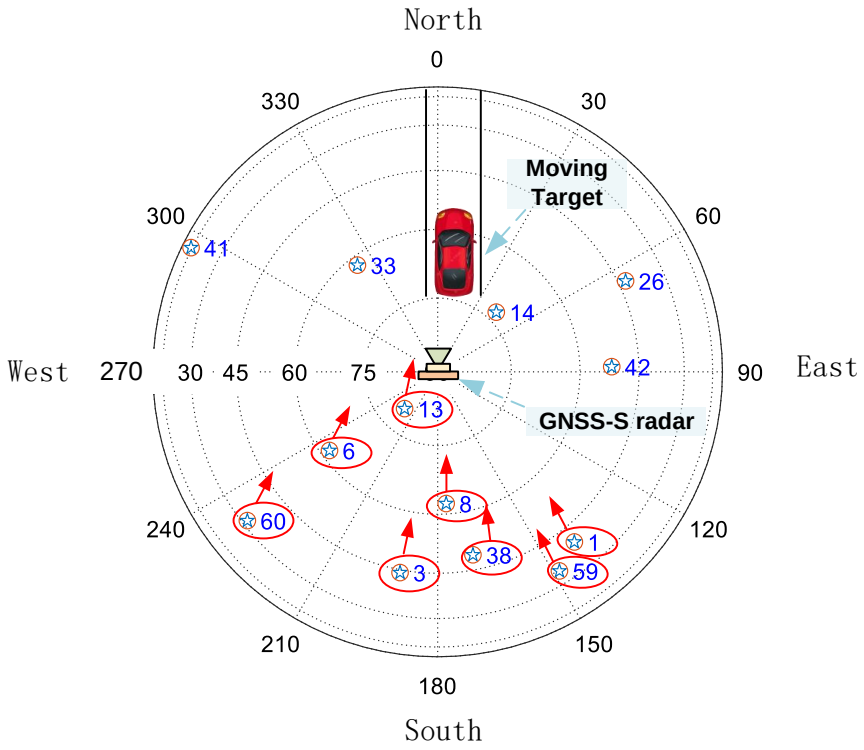

Figure 14. BDS satellite distribution and relative position.

Table 3. Position information of eight satellites.

Satellite Number	Elevation /°	Azimuth/°
1	35	140
3	44	189
6	62	234
8	69	166
13	80	222
38	49	169
59	39	146
60	32	232

Figure 15 shows the original data after signal BEC processing. Since the navigation satellite signal scattered by the car is extremely weak, the target trajectory cannot be directly observed before accumulation in the slow time direction.

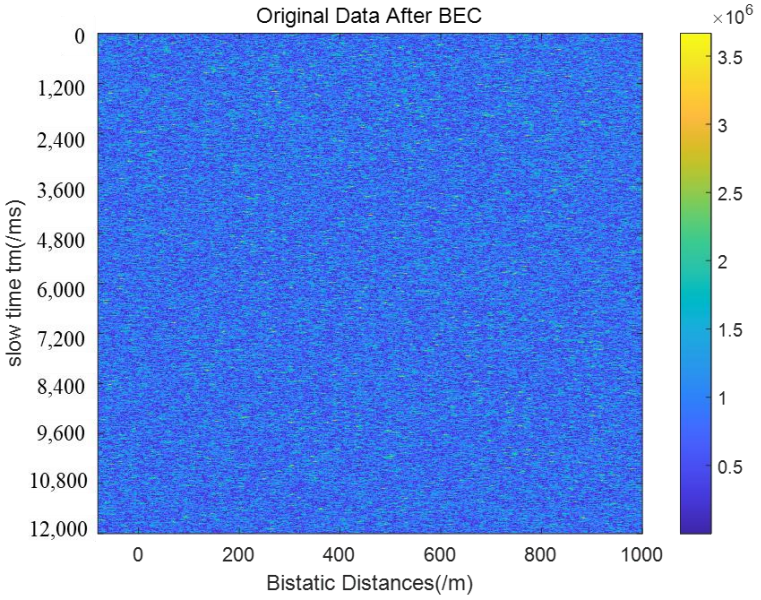

Figure 15. Original data after BEC processing.

After long-term coherent accumulation of the scattered signals of the eight navigation satellites using the method proposed in this paper, the accumulated results in the "time-distance domain" are shown in Figure 16. The vertical axis is the slow time tm, and the horizontal axis is the vehicle movement distance R. It can be seen from the figure that the signal moves in the distance direction with the passage of slow time, corresponding to the trajectory of the car.

In the echo track diagram of the 8 satellites, three moments (t1, t2, and t3) were taken to compare and analyze the signal intensity of the target echo, as shown in Figure 17. Since the position of the eight BDS satellites are different, and the bistatic angles formed by the receivers are also different, the target echo track formed by a single BDS satellite is different. In addition, because the car is in motion, there will be a discontinuous state of echo energy in a single track.

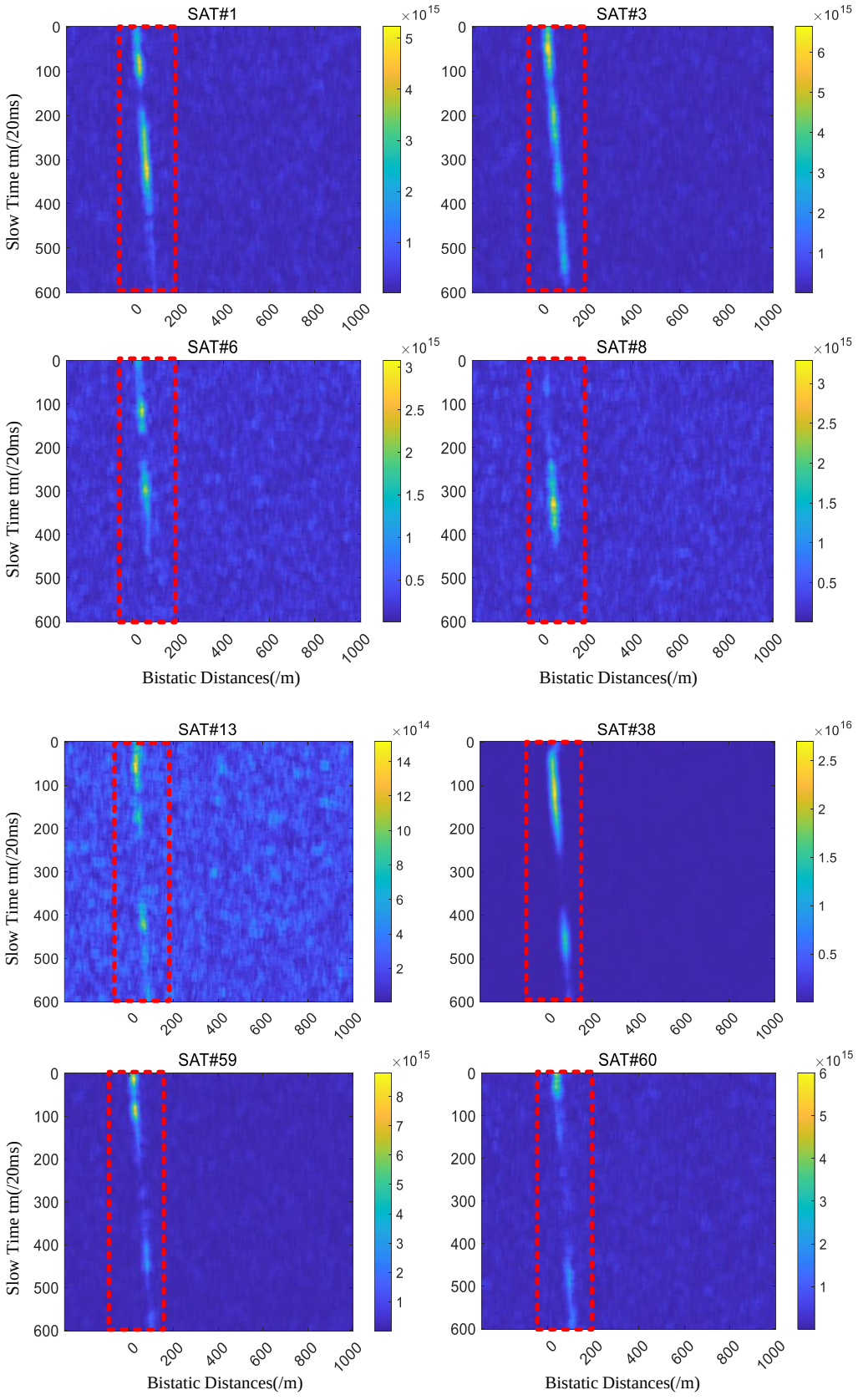

Figure 16. Trajectories of target echoes from 8 satellites.

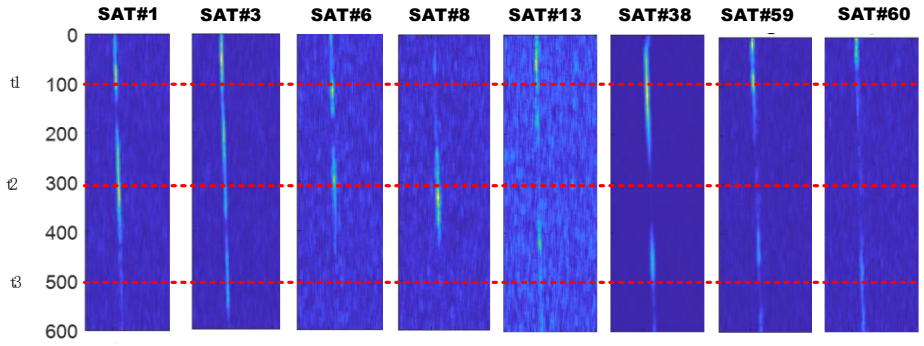

Figure 17. Comparison of the echo intensity of 8 satellites.

The intercepted signal energy distribution of the eight satellites is drawn as a two-dimensional diagram, as shown in Figure 18. The RCS of different angles of the car is different, so the echo signal intensity is also different. The echo signal intensity of the 38th satellite is the largest, and the echo signal intensity of the 13th satellite is the smallest. This is mainly due to the fact that the azimuth angle and elevation angle of the satellites are different, therefore the bistatic RCS formed by the car is different.

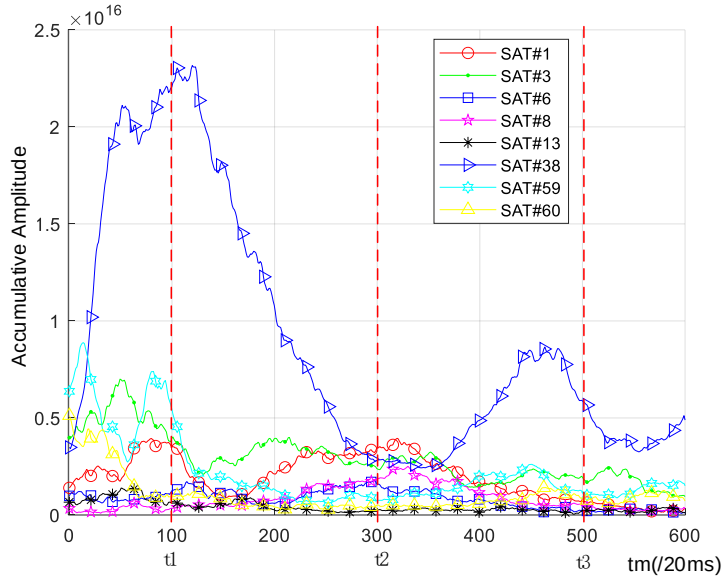

Figure 18. Signal energy distribution and comparison of 8 satellites.

In order to make full use of the scattering signals of multiple satellites and obtain stable echoes, the trajectory diagrams of the eight navigation satellites in Figure 16 are given weighted accumulation to form the motion trajectory diagram shown in Figure 19. The continuity and intensity of the signal are significantly improved compared with the single satellite state in Figure 16. As shown in Table 4, the proportion of time when a single satellite echo signal is detected ranges from 32% to 67%, and the signal echo trajectory is discontinuous. After the eight satellite echoes are fused, a continuous echo signal track can be obtained.

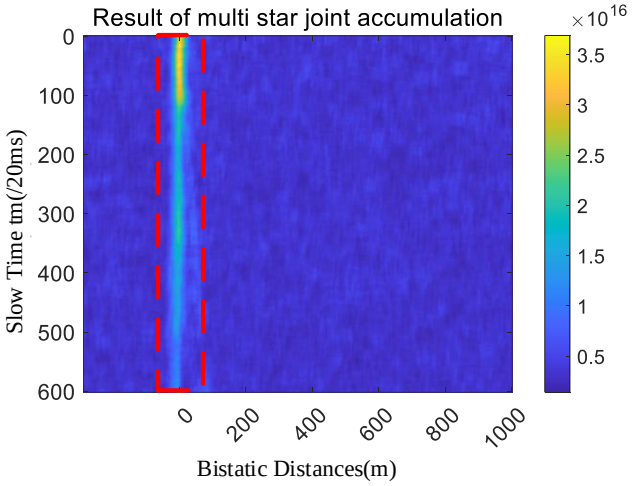

Figure 19. The target signal trajectory of the fusion of eight satellites.

Table 4. Comparison before and after the combination of 8 satellite signals.

Satellite Number	Time Proportion of Detected Echo	SNR
1	58%	13.4
3	67%	14.1
6	47%	11.6
8	32%	11.9
13	37%	8.7
38	55%	18.2
59	35%	15.6
60	34%	14.4
Joint result of 8 satellites	100%	19.5

In addition, Table 4 lists the highest SNR of echo signals before and after fusion. After fusion, the maximum SNR does not increase much, mainly because the weighted fusion method is used to enhance the fusion of weak signals and suppress the excessive growth of strong signals.

Finally, the signal in Figure 19 is accumulated again according to the slow time tm to form the result in Figure 20a. The car target presents an obvious energy accumulation peak in the figure. Figure 20b is a graph showing the relationship between frequency and cumulative energy value. It can be seen from the figure that the Doppler frequency shift of the signal is compensated to zero, and the signal energy has a good concentration effect.

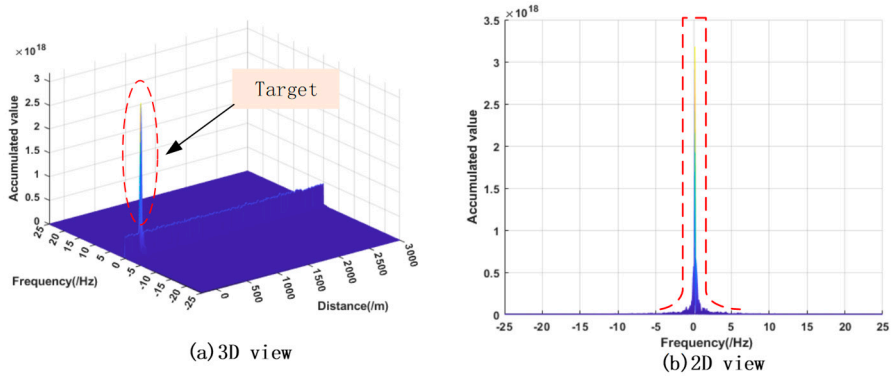

Figure 20. Target Energy Accumulation.

5. Discussion

In the present research, the continuous detection of extremely weak GNSS echo signals of moving targets is processed from two aspects: single-satellite echo signal accumulation and multi-satellite joint processing. In the aspect of single-satellite echo signal processing, the SNR of weak signals is improved by long-term coherent integration from the aspect of improving signal phase consistency. Firstly, the target scattering signal is compressed according to the direct reference signal, and the influence of satellite Doppler and navigation bits on phase is eliminated. Then, for the residual Doppler brought by the target motion, the phase is differentiated twice to remove the impact of the residual Doppler of the target motion on the phase, and then the above corrected signals are coherently accumulated. This method can improve the phase consistency of the signal, increase the accumulated gain, and suppress noise.

The Doppler frequency of the GNSS scattering echo signal is caused by satellite motion and target motion. The Doppler effect caused by satellite motion needs to be removed by means of direct signal. The Doppler estimation accuracy of the direct satellite signal will affect the carrier rejection effect of the scattered echo signal. In practical application, a high-precision carrier tracking loop should be used to achieve accurate measurement of the direct carrier.

The Doppler effect caused by target motion is irregular. It is necessary to eliminate the Doppler effect of target motion for long time accumulation. The common Radon–Fourier transform method needs to search the range and Doppler jointly. Because the GNSS signal is a continuous signal, the calculation is very large. However, the method in this paper can greatly simplify the calculation and obtain a good accumulation effect. The comparison of SNR after processing between this method and traditional coherent and incoherent accumulation methods is shown in Figure 21, which shows the SNR obtained by the three methods at different accumulation times.

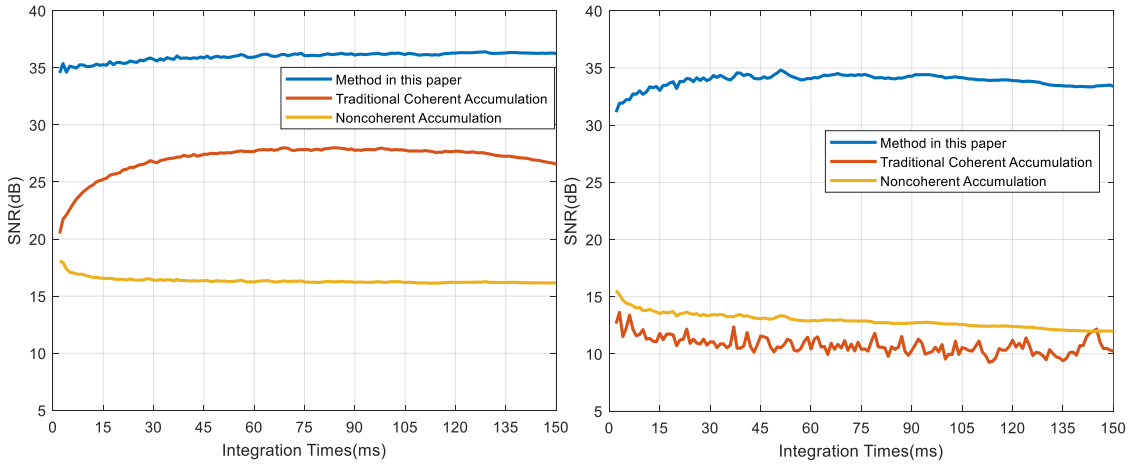

(**a**) The target speed is 3 m/s (**b**) The target speed is 100 m/s

Figure 21. SNR of three methods.

Figure 21a shows the accumulation effect when the target moving speed is 3 m/s. It can be seen that when the speed is low, the coherent accumulation effect is better than the noncoherent accumulation effect because the signal phase changes less during the integration time. Figure 21b shows the accumulation effect when the moving speed is 100 m/s. It can be seen that when the moving speed of the target increases, the effect of noncoherent accumulation is better than that of coherent accumulation. This is mainly due to the large phase change caused by the target movement, and the large signal phase difference in one accumulation period counteracts the accumulation effect.

However, of the three methods, the method proposed in this paper is better than the cumulative gain of the other two methods. Especially for high-speed moving targets, the

gain improvement effect of this method is more obvious, and the coherent cumulative gain is greatly improved, which shows the superior performance of this method.

In the aspect of multi-satellite joint processing, eight satellite echo signals are used for joint processing in this paper, which improves the continuity of signal echo signals, as shown in Table 4. It can effectively overcome the echo interruption caused by the change in single-satellite bistatic RCS characteristics. However, in this paper, the joint of multi-satellite echo signals is realized by means of weighted addition, and the signal weights are manually set according to the signal intensity. Further research on the signal fusion method will be able to obtain a better signal joint effect.

6. Conclusions

GNSS-based moving target detection has broad application prospects, but the main problems are that (1) the GNSS signal power is extremely low and the pseudo-random code and navigation message are modulated on the carrier; (2) the movement of the target will cause the change in signal phase and the migration of signal amplitude; and (3) single-satellite bistatic RCS has scintillation problems during target movement, which causes discontinuous echo energy. This paper proposes a new amplitude-phase self-correction GNSS-S signal accumulation method to realize the detection of moving targets. Firstly, the block expansion compression and phase differential method are used for the echo signal of a single satellite to increase the coherent cumulative gain; then, the signal amplitude of multiple satellites is corrected, and the multi-satellite weighted accumulation is used to improve the continuity and SNR of the echo signal. The effectiveness of the method is verified by simulation and field test, and compared with the traditional coherent accumulation and non-coherent accumulation methods, the superiority of the proposed method is verified, and the effect is more significant in the accumulation of scattering signals of high-speed moving targets. Finally, through the method proposed in this paper, the gain and continuity of the echo signal of moving weak and small targets are improved, and the detection of moving targets based on GNSS passive radar is realized. It will be extended to spaceborne applications in the future, which will generate even greater value.

Author Contributions: W.G. and Z.X. implemented the methods and conceived and designed the experiments; F.Y. supervised the research; X.L., C.Z., and Z.L. performed the experiments; S.J. put forward valuable suggestions; Y.Z. (Yao Zhang), Z.Z., T.Z. and Y.Z. (Ying Zhang) analyzed part of the data; and W.G. wrote the paper. All authors have read and agreed to the published version of the manuscript.

Funding: This research received no external funding. It was carried out by the State Key Laboratory of Space-Earth Integrated Information Technology with self-financing.

Data Availability Statement: The data presented in this study are available on request from the corresponding author. The data are not publicly available due to intellectual property protection.

Conflicts of Interest: The authors declare no conflict of interest.

References

1. Yan, Q.; Huang, W. Sea ice remote sensing using GNSS-R: A review. *Remote Sens.* **2019**, *11*, 2565. [CrossRef]
2. Liu, J.; Shao, L.; Zhang, X. Advances in GNSS-R studies and key technologies. *Geomat. Inf. Sci. Wuhan Univ.* **2007**, *32*, 955–960.
3. Ma, H.; Antoniou, M.; Cherniakov, M.; Pastina, D.; Santi, F.; Pieralice, F.; Bucciarelli, M. Maritime target detection using GNSS-based radar: Experimental proof of concept. In Proceedings of the 2017 IEEE Radar Conference(RadarConf), Seattle, WA, USA, 8–12 May 2017; pp. 0464–0469.
4. Cherniakov, M.; He, X.; Zeng, T. Signal detectability in SS-BSAR with GNSS non-cooperative transmitter. *IEE Proc. -Radar Sonar Navig.* **2005**, *152*, 124–132.
5. Pastina, D.; Santi, F.; Pieralice, F.; Bucciarelli, M.; Ma, H.; Tzagkas, D.; Antoniou, M.; Cherniakov, M. Maritime moving target long time integration for GNSS-based passive bistatic radar. *IEEE Trans. Aerosp. Electron. Syst.* **2018**, *54*, 3060–3083. [CrossRef]
6. Pastina, D.; Sedehi, M.; Cristallini, D. Passive bistatic ISAR based on geostationary satellites for coastal surveillance. In Proceedings of the 2010 IEEE Radar Conference, Arlington, VA, USA, 10–14 May 2010; pp. 865–870.
7. He, Z.; Yang, Y.; Chen, W. A hybrid integration method for moving target detection with GNSS-based passive radar. *IEEE J. Sel. Top. Appl. Earth Obs. Remote Sens.* **2020**, *14*, 1184–1193. [CrossRef]

8. Li, Y.; Yan, S.; Gong, J.; Zeng, F. SNR enhancement of back scattering signals for bistatic radar based on beidou GEO satellites. *Remote Sens.* **2021**, *13*, 1254. [CrossRef]
9. Xu, J.; Yu, J.; Peng, Y.-N.; Xia, X.-G. Radon-Fourier transform for radar target detection, I: Generalized Doppler filter bank. *IEEE Trans. Aerosp. Electron. Syst.* **2011**, *47*, 1186–1202. [CrossRef]
10. Chen, X.; Guan, J.; Liu, N.; He, Y. Maneuvering target detection via Radon-fractional Fourier transform-based long-time coherent integration. *IEEE Trans. Signal Process.* **2014**, *62*, 939–953. [CrossRef]
11. Xu, J.; Yan, L.; Zhou, X.; Long, T.; Xia, X.-G.; Wang, Y.-L.; Farina, A. Adaptive Radon–Fourier Transform for Weak Radar Target Detection. *IEEE Trans. Aerosp. Electron. Syst.* **2018**, *54*, 1641–1663. [CrossRef]
12. De Luca, A.; Daniel, L.; Gashinova, M.; Cherniakov, M. Target parameter estimation in moving transmitter moving receiver forward scatter radar. In Proceedings of the International Radar Symposium, Prague, Czech Republic, 28–30 June 2017; IEEE Computer Society: Washington, DC, USA, 2017; pp. 1–7.
13. Gao, W.; Yue, F.; Tang, D.; Liu, P. Research on GNSS Navigation Method of Lunar Orbiting Spacecraft Based on Ground Enhancement. In Proceedings of the China Satellite Navigation Conference (CSNC 2022) Proceedings, Beijing, China, 25–27 May 2022; Springer: Singapore, 2022; pp. 563–572.
14. Gao, W.; Yue, F.; Xu, Z. Integrity Monitoring Methods of Beidou Receiver Based on Inertial Assistance. *Navig. Position. Timing* **2021**, *8*, 107–113.
15. Carlson, B.; Evans, E.; Wilson, S. Search radar detection and track with the Hough transform. II. Detection statistics. *IEEE Trans. Aerosp. Electron. Syst.* **1994**, *30*, 109–115. [CrossRef]
16. Cha, C.-C.; Michels, J.; Starczewski, E. An RCS analysis of generic airborne vehicles dependence on frequency and bistatic angle. In Proceedings of the 1988 IEEE National Radar Conference, Ann Arbor, MI, USA, 20–21 April 1988; pp. 214–219. [CrossRef]
17. Stephan, S.R.; Thuringian, M.A.H. Simulations and Measurements of the Bistatic Radar Cross Section of Vulnerable Road Users between 2 GHz and 6 GHz. In Proceedings of the 2018 IEEE MTT-S International Conference on Microwaves for Intelligent Mobility (ICMIM), Munich, Germany, 15–17 April 2018; pp. 1–4. [CrossRef]
18. Myint, S.J.; Schneider, C.; Röding, M.; Galdo, G.D.; Thomä, R.S. Statistical Analysis and Modeling of Vehicular Radar Cross Section. In Proceedings of the 2019 13th European Conference on Antennas and Propagation (EuCAP), Krakow, Poland, 31 March–5 April 2019; pp. 1–5.
19. Abdul Aziz, N.H.; Raja Abdullah, R.S.A.; Abdul Rashid, N.E.; Hashim, F. RCS Predictions through Angle of Ground Moving Target using LTE-Based Passive Forward Scattering Radar. *J. Telecommun. Electron. Comput. Eng. (JTEC)* **2017**, *9*, 129–132.
20. Xie, Z.; Yue, H.; Cao, Y. A RCS prediction method for multipath effect of the ground plane. In Proceedings of the 2017 International Applied Computational Electromagnetics Society Symposium (ACES), Suzhou, China, 1–4 August 2017; pp. 1–4.
21. China Satellite Navigation Office. BeiDou Navigation Satellite System Signal In Space Interface Control Document Open Service Signal B3I (Version 1.0). Available online: http://en.beidou.gov.cn/SYSTEMS/ICD/ (accessed on 7 February 2023).